Exploring the Flexibility of Ribosome Recycling Factor Using Molecular Dynamics

Scott M. Stagg and Stephen C. Harvey
Department of Biology, Georgia Institute of Technology, Atlanta, Georgia 30332

ABSTRACT Ribosome recycling factor is proposed to be flexible, and that flexibility is believed to be important to its function. Here we use molecular dynamics to test the flexibility of *Escherichia coli* RRF (ecRRF) with and without decanoic acid bound to a hydrophobic pocket between domains 1 and 2, and *Thermus thermophilus* RRF (ttRRF) with and without a mutation in the hinge between domains 1 and 2. Our simulations show that the structure of ecRRF rapidly goes from having an interdomain angle of 124° to an angle of 98° independently of the presence of decanoic acid. The simulations also show that the presence or absence of decanoic acid leads to changes in ecRRF flexibility. Simulations of wild-type and mutant ttRRF (R32G) show that mutating Arg-32 to glycine decreases RRF flexibility. This was unexpected because the range of dihedral angles for arginine is limited relative to glycine. Furthermore, the interdomain angle of wild-type *T. thermophilus* goes from 81° to 118° whereas the R32G mutant remains very close to the crystallographic angle of 78°. We propose that this difference accounts for the fact that mutant ttRRF complements an RRF deficient strain of *E. coli* whereas wild-type ttRRF does not. When the ensemble of RRF structures is modeled into the ribosomal crystal structure, a series of overlaps is found that corresponds with regions where conformational changes have been found in the cryoelectron microscopic structure of the RRF/ribosome complex, and in the crystal structure of a cocomplex of RRF with the 50S subunit. There are also overlaps with the P-site, suggesting that RRF flexibility plays a role in removing the deacylated P-site tRNA during termination of translation.

INTRODUCTION

After termination of translation in prokaryotes, the complex of the 70S ribosome, deacylated tRNA, and mRNA (the posttermination complex) must be broken down into individual components, or recycled, before translation can begin again. This reaction is in part catalyzed by ribosome recycling factor (RRF) (reviewed in Janosi et al. (1) and Nakamura and Ito (2)). An essential gene in *Escherichia coli* (3), RRF binds to the posttermination complex along with EF-G and GTP and helps recycle the translational components in a GTP-dependent manner.

The detailed mechanism for RRF action is unclear. One model for how RRF participates in ribosome disassembly proposes that RRF works in a similar manner to tRNAs, binding to the A-site, and then being translocated to the P-site by EF-G and GTP hydrolysis (4). In this model, translocation of RRF ejects the deacylated tRNA and mRNA, and the disassembly of the 70S is later completed by IF3. In the second model, RRF along with EF-G splits the 70S into the 30S and 50S, leaving the mRNA and P-site tRNA bound to the 30S (5).

The first crystal structure solved for RRF revealed it to have a geometry similar to that of tRNA (6) with two domains (domains 1 and 2) spaced ~90° from each other. This led to the suggestion that RRF is a tRNA mimic. Recent studies, however, have shown that RRF binds to the ribosome in a different location than tRNAs. Hydroxyl radical probing by Lancaster et al. (7) indicated that RRF binds the ribosome near the interface between the large and small subunits in an orientation never observed for tRNAs. This orientation was essentially confirmed in a cryoelectron microscopy (cryo-EM) study that determined the structure of RRF bound to the ribosome at 12 Å resolution (8), although these authors did find some differences in the positions from cryo-EM versus those predicted by hydroxyl radical probing. They found that RRF lies along the subunit interface with domain 1 overlapping the A- and P-sites, and the tip of domain 2 close to the decoding site. It interacts primarily with those parts of the 23S (large subunit) rRNA that form intersubunit bridges B2a and B3. Both the hydroxyl radical probing and cryo-EM studies suggest that the mechanism of RRF recycling involves more than simple tRNA mimicry. Both studies were performed in the absence of EF-G, however, and it is possible that RRF changes conformation after EF-G binds, or that RRF mimics tRNA in later stages of recycling. RRF has recently been crystallized with the large ribosomal subunit from *Deinococcus radiodurans* (9). The crystal structure is consistent with the cryo-EM studies on RRF in the intact ribosome, although RRF is rotated ~7° and translated ~1.5 Å, leading to the suggestion that RRF primes the intersubunit bridge B2a for the action of EF-G (9).

Crystal structures have been determined for RRF isolated from several different species (6,10–12). The fold of RRF in all these structures is very similar. The structure is comprised of two domains connected by two loops (Fig. 1 *A*). Domain 1 consists of a three-helix bundle whereas domain 2 is a $\beta/\alpha/\beta$ sandwich. The relative orientation of domains 1 and 2 differs substantially between the various structures. For example, the structure from *Thermatoga maritima* (6) shows the interdomain angle to be 95°, whereas RRF from *E. coli* in

Submitted September 3, 2004, and accepted for publication July 5, 2005.
Address reprint requests to Scott M. Stagg, sstagg@scripps.edu.

0006-3495/05/10/2659/08 $2.00
doi: 10.1529/biophysj.104.052373

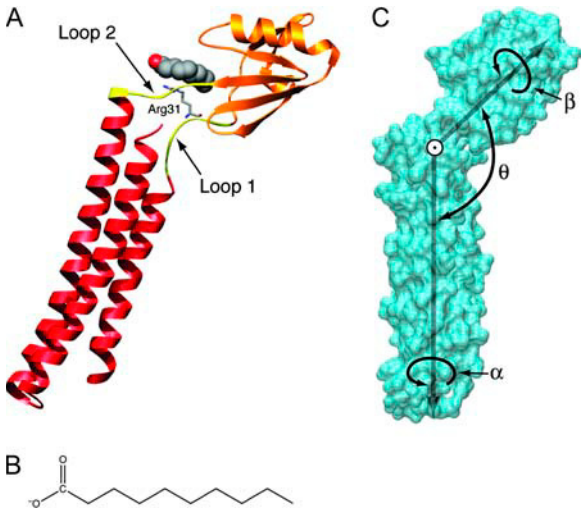

FIGURE 1 The structure of *E. coli* RRF and decanoic acid. (*A*) Domain 1 (*red*) of RRF is connected to domain 2 (*orange*) by two loop regions (*yellow*). Decanoic acid (*spheres*) is bound to a hydrophobic pocket in domain 2. Arg-31, which is homologous to Arg-32 in ttRRF, is shown as sticks. (*B*) Chemical structure of decanoic acid. (*C*) Rotational degrees of freedom when domains 1 and 2 are treated as rigid bodies; θ is the interdomain bend angle, α is the rotation of domain 2 around domain 1, and β is the rotation of domain 1 around domain 2.

complex with the detergent decyl-β-D-maltopyranoside (10) has an angle of 124°. The fact that the interdomain orientation differs so much between the structures has lead to the suggestion that RRF is flexible, and that the flexibility may be important to RRF function.

Various other studies have suggested that the loops connecting domain 1 and 2 of RRF act as a flexible hinge. In one study, expressing *T. maritima* RRF in *E. coli* inhibited the growth of the host cells (13). It was suggested that this might be because *T. maritima* RRF is less flexible at 37°C than at the native temperature of 80°C. Like *T. maritima* RRF, *Thermus thermophilus* RRF is incapable of complementing a temperature sensitive mutation of RRF in *E. coli* (14). Another study showed that mutating residues in loop 1 or loop 2 of *T. thermophilus* RRF conferred on it the ability to complement temperature-sensitive *E. coli* RRF and suggested that the mutations increased RRF flexibility (12). Finally, a crystal structure of RRF from *E. coli* was solved in complex with a detergent molecule, decyl-β-D-maltopyranoside (an agent added during crystallization), that binds a hydrophobic cleft in domain 2 and appears to stabilize RRF in an open conformation (10). These authors suggested that RRF is capable of large interdomain motions, and that the detergent stabilizes RRF in the open conformation, inhibiting RRF flexibility in vivo.

The flexibility of RRF was measured directly by Yoshida et al. (15). Using NMR and molecular dynamics (MD) simulations, they showed that domains 1 and 2 undergo characteristic interdomain reorientations on the nanosecond timescale. In their 4.5-ns simulation, they observed domain 2 to undergo an 11° rotation around the axis of the three-helix bundle comprising domain 1. However, because their simulation was limited to 4.5 ns, only the lower limit of domain motions was observed.

Here we report further investigations of RRF flexibility using molecular dynamics simulations. We performed 20-ns simulations of RRF from *E. coli* (ecRRF), with and without decanoic acid, which we used as a substitute for the crystallographic detergent molecule. We also simulated wild-type *T. thermophilus* RRF (ttRRF) and a mutant where we changed Arg-32 to glycine (ttRRF_R32G). We analyzed the simulations for interdomain motions. These studies show that RRF undergoes large interdomain motions on a nanosecond timescale. They also show that the presence of the detergent molecule in ecRRF or mutation of residue 32 of ttRRF results in changes in both RRF conformation and flexibility. We also examine what these results imply for the function of RRF on the ribosome.

METHODS

Molecular dynamics

Simulations were performed using the NAMD software package (16) run on 60 2.67 GHz Intel Xeon processors of our in-house Linux cluster. Each simulation ran for ~180 h of CPU time. The simulations were run for 20 ns, except for ttRRF and ttRRF_R32G, which were run for 19.6 ns.

The proteins were simulated using the CHARMM22 force field (17). Because there are no parameters for decyl-β-D-maltopyranoside in any of the CHARMM force fields, the detergent molecule in ecRRF/DEC was modeled as decanoic acid. Decanoic acid was parameterized based on palmitic acid in the CHARMM27 lipid force field by removing six methylene groups from palmitic acid. Each protein was solvated in a periodic box of TIP3 water. Electrostatics were calculated using the particle mesh Ewald method (18). Simulations were carried out in the constant pressure and temperature regime using the Berendsen method (19). Bonds were held rigid using the SHAKE algorithm, allowing for a time step of 2 fs. The simulations were equilibrated by ramping the temperature 10 K every picosecond from 30 to 300 K over 20 ps, after which the temperature was held at 300 K for 180 ps. The mutation of Arg-32 of ttRRF to glycine was accomplished using the psfgen program in the NAMD package by simply substituting glycine for arginine at that position in the structure.

Angle definitions

The three angles describing intramolecular RRF motions were determined as follows. The hinge point is defined by the center of mass of residues 30, 31, 104, and 105. The long axis of each domain is defined by connecting the hinge to a point at the other end of the domain; for ecRRF, the center of mass of residues 5, 139, and 156 defines the tip of domain 1, whereas the tip of domain 2 is defined by the center of mass of residues 51, 56, 68, 78, and 98. Centers of mass of homologous residues were used to define the tips of the two domains in ttRRF and ttRRF_R32G. The bend angle between the two domains, θ, is simply the dot product of unit vectors along the two domain axes; α was calculated by superposing domain 2 in each frame of the trajectory onto domain 2 of the crystal structure of ecRRF, then measuring the angle between the instantaneous axis of domain 1 and the plane defined by the two axes in the first frame. For both sets of simulations of ecRRF and ttRRF, the proteins were superposed on the crystal structure of ecRRF so that the angles could be compared relative to a standard orientation; β, the angle for rotations of domain 1 around domain 2, was determined similarly.

Model of RRF in situ

To examine the functional implications of RRF flexibility, we generated an ensemble of models for RRF in the 70S ribosome. We began by superposing the *Deinococcus* 50S subunit from the RRF/50S crystal structure (9) onto the 50S subunit from the crystal structure of the *Thermus thermophilus* 70S ribosome (20). This places domain 1 of RRF into the *Thermus* ribosome. We then positioned each frame of the MD simulation by superposing domain 1 from the simulation onto domain 1 of the RRF/ribosome model, generating an ensemble of structures that suggests possible interactions generated by the thermal fluctuations. Next we superposed full-length protein for both ecRRF and ttRRF onto domain 1 of the RRF/ribosome model. We then generated a second ensemble by using domain 2 of the newly docked protein for the superposition of each frame of the simulation onto the RRF/ribosome model.

RESULTS

Simulations of ~20 ns were performed on each of the following: ecRRF, ecRRF in complex with decanoic acid (ecRRF/DEC), wild-type ttRRF, and ttRRF with Arg-32 mutated to glycine (ttRRF_R32G). For the simulation of ecRRF, the starting structure was simply the protein component of the crystal structure of ecRRF in complex with decyl-β-D-maltopyranoside (10). No additional cofactors were included in this simulation. For ecRRF/DEC, decanoic acid (Fig. 2 *B*) was substituted for decyl-β-D-maltopyranoside because decyl-β-D-maltopyranoside is not parameterized in any of the common force fields. Decanoic acid was chosen because its acyl chain is the same length as that of decyl-β-D-maltopyranoside, and decanoic acid could be parameterized based on other fatty acids (see Methods). The starting structure of ttRRF was identical to the ttRRF crystal structure (12). For the ttRRF mutant, we modified the ttRRF crystal structure, mutating Arg-32 to glycine. In each simulation, the protein was solvated in a periodic water box and simulated at constant temperature and pressure. The subsequent trajectories were analyzed for collective domain motions.

For all the simulations, domains 1 and 2 remain intact through the course of the simulations. The stability of each domain was examined by superposing each domain of each frame of the trajectory onto itself in the first frame. The average root mean square deviation (RMSD) is 2–3 Å for both domains 1 and 2. Thus, to a first approximation, each domain moves as a rigid body.

We measured the degree of collective domain motion by defining angles for three types of domain motions (Figs. 1 *C* and 2, *center* panel). Briefly, a hinged body with two rigid domains has three internal degrees of freedom, whose definitions are aided by defining two axes that intersect at the hinge point, one axis for each domain. The first degree of freedom, the bend angle θ, corresponds to the angle between the two axes. The second, α, can be thought of in either of two ways. If subunit 2 is considered fixed, α describes the rotation of subunit 1 about its long axis. If subunit 1 is

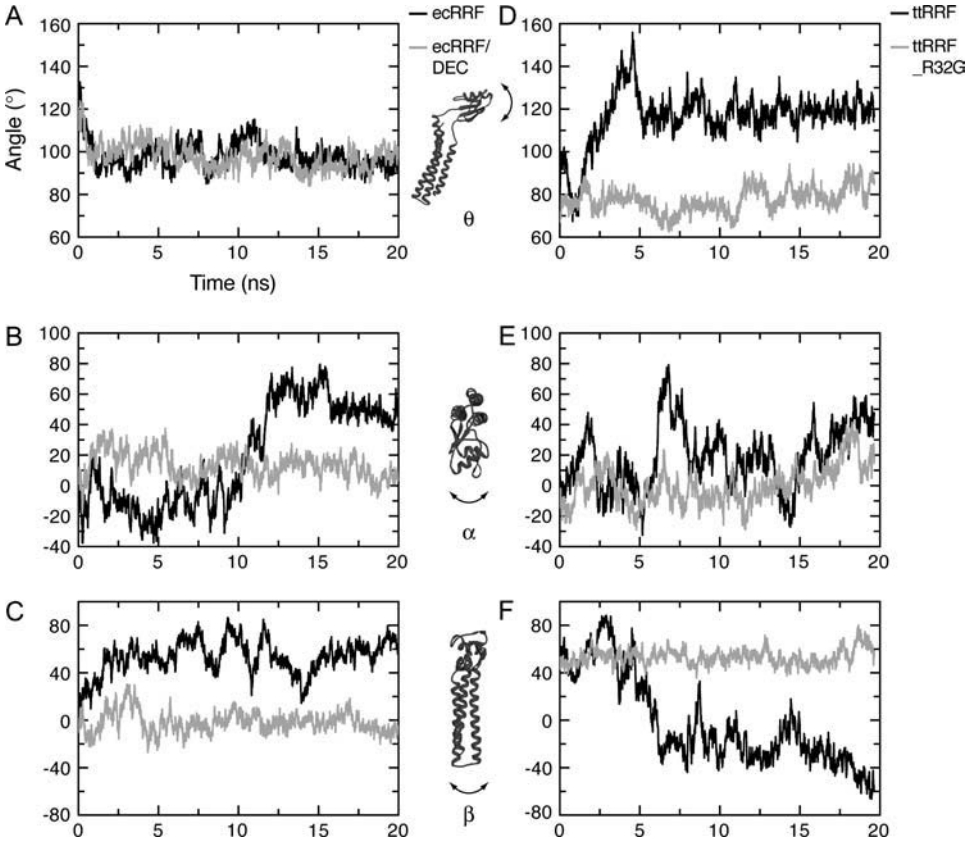

FIGURE 2 Domain motions of ecRRF and ttRRF. The three types of domain motions measured are indicated in the center panels (*blue ribbons*). Panels *A–C* are measurements of the ecRRF (*black*) and ecRRF/DEC (*blue*) angles whereas panels *D* and *F* are measurements of ttRRF (*black*) and ttRRF_R32G (*blue*). Panels *A* and *D* are measurements of the angle between domains 1 and 2. Panels *B* and *E* are measurements of rotations of domain 2 around domain 1. Panels *C* and *F* are measurements of rotations of domain 1 around domain 2.

considered fixed, α describes the rotation of subunit 2 about subunit 1, a sort of waggling motion that carries subunit 2 out of the plane defined by the original pair of axes. The schematic for α in the center panel of Fig. 2 shows the latter definition. Similarly, the third degree of freedom describes rotations of domain 2 about its long axis, or, alternatively, the rotation of domain 1 relative to domain 2 (β in Fig. 2). The analyses for these three types of angular motion are summarized in Table 1, and movies of the domain motions for each of the simulations are provided in the Supplementary Material.

Changes in the interdomain angle θ

First we calculated the bend angle, θ, between domains 1 and 2. In the ecRRF crystal structure, this angle is 124°. After 1 ns in the simulations of both ecRRF and ecRRF/DEC, the angle went to an equilibrium value of 98° (Fig. 2 *A*). This is surprising, because one would assume that the crystal structure is very close to the equilibrium structure. The standard deviation of the angle is 5.4° for both ecRRF and ecRRF/DEC, indicating that the two proteins are equally flexible in this degree of freedom.

The same analysis was performed for the simulations of ttRRF. Over the course of the first 5 ns, the interdomain angle of wild-type ttRRF gradually increased from the crystallographic value of 81° to an equilibrium value of 118° (Fig. 2 *D*). The bend angle for the mutant ttRRF, on the other hand, stayed very close to the crystallographic value. This result was surprising, as one would expect the mutant rather than the wild type to change from the crystallographic conformation. The standard deviation of the interdomain angle for wild-type ttRRF after the first 5 ns is 5.3 Å, whereas the standard deviation for ttRRF_R32G is 6.3 Å. This indicates that once wild-type ttRRF has reached its optimal bend angle of ~118°, it is modestly less flexible in this degree of freedom than is ttRF_R32G.

Rotations of domain 2 around domain 1 (α)

The second degree of freedom describes rotations around the long axis of domain 1. ecRRF samples two conformations for this type of rotation, one around $\alpha = -10°$ and one near $\alpha = 50°$ (Fig. 2 *B*). For ecRRF/DEC, the angle oscillates around 13°. These results suggest that the presence of decanoic acid reduces the conformational variability of RRF by favoring the 13° angle. ttRRF shows a high degree of flexibility for this type of rotation. It samples angles as low as −39° and as high as 80° (Fig. 2 *E*). Compared to ttRRF, the flexibility of ttRRF_R32G is reduced for this degree of freedom, with values of α ranging from −32° to 43°.

TABLE 1 Average angles and standard deviations for the different domain motions in the RRF simulations

	ecRRF		ecRRF/DEC		ttRRF		ttRRF_R32G	
	Average	±SD	Average	±SD	Average	±SD	Average	±SD
θ	98.0	6.5	97.8	5.9	116.3	12.4	77.5	5.7
					118.4*	5.3*	77.4*	6.3*
α	19.3	33.1	13.4	8.6	18.7	20.4	−0.1	12.5
β	53.2	14.2	−1.7	8.8	−1.9	37.7	53.2	6.6

*Measurements excluding the first 5 ns.

Rotations of domain 1 around domain 2 (β)

The third degree of freedom corresponds to rotations around the long axis of domain 2. For this rotation, ecRRF was once again highly mobile, with large fluctuations around an average value of $\beta = 53°$ (Fig. 2 *C*). ecRRF/DEC was less mobile and stays very close to the crystallographic value with an average angle of −1.7°. This suggests that decanoic acid stabilizes the crystallographic conformation for this type of domain motion. Like ecRRF, ttRRF is also highly mobile for this motion. It starts with an angle of 49°, then, after ~5 ns, goes to an angle of ~−16°, and finally ends at an angle of −60°. For ttRRF_R32G, on the other hand, β stays very close to the crystallographic value of 53°. The R32G mutation stabilizes the conformation at $\beta = 53°$ and reduces the flexibility for this motion.

Overall flexibility

The global flexibility of the proteins was measured by calculating the average structure for each simulation and then superposing each frame onto the average structure and calculating the RMSD (Fig. 3). ecRRF requires ~5 ns to reach equilibrium values of α, β, and θ, (Fig. 2), so the first 5 ns of the simulation were excluded from the calculation of the average structure of ecRRF. ecRRF and ecRRF/DEC fluctuate around average RMSDs of 3.95 and 3.86 Å, respectively (Fig. 3 *A*), whereas ttRRF and ttRRF_R32G fluctuate around RMSDs of 2.74 and 2.30 Å (Fig. 3 *B*). The standard deviations of the RMSDs for ecRRF and ecRRF/DEC differ significantly. The standard deviation for ecRRF is 0.76 Å whereas the standard deviation for ecRRF/DEC is 0.49 Å, indicating that ecRRF is globally more flexible than ecRRF/DEC. The standard deviations of ttRRF and ttRRF_R32G are 0.68 and 0.58 Å, respectively, indicating that ttRRF is moderately more flexible than ttRRF_R32G.

DISCUSSION

We have characterized the flexibility of RRF and how different mutations and cofactors affect RRF conformation and flexibility. The most significant experimental data against which our simulations might be compared are from the NMR relaxation experiments carried out by Yoshida et al. (15) on *E. coli* RRF. Those authors attempted to develop a unified view of intramolecular motions in RRF by comparing their NMR data with the results of a 4.5-ns MD simulation.

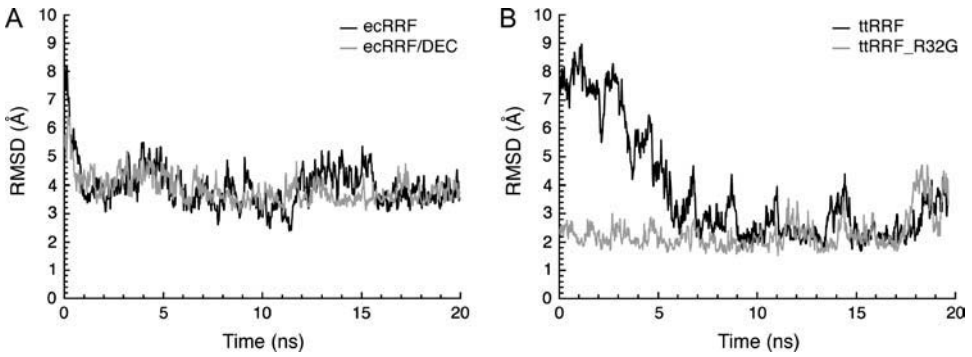

FIGURE 3 RMSD of RRF simulations to average structure. Panel *A* shows the RMSDs of ecRRF (*black*) and ecRRF/DEC (*blue*). Panel *B* shows the RMSDs of ttRRF (*black*) and ttRRF_R32G (*blue*).

They admitted a number of difficulties with the analysis of their NMR data, which precludes a rigorous quantitative comparison of our results with theirs, but the qualitative comparisons are quite interesting.

We begin by considering the problems that Yoshida et al. (15) encountered in analyzing their NMR data. They found that the motions were too complex to be analyzed by the model-free approach often used in such NMR experiments, stating that ''the quality of fit in (the) simple model-free approach is poor.'' They attempted to generate relaxation data at multiple field strengths, an approach that had been successfully used by others to tease out complex intramolecular motions (21,22). Unfortunately, experimental problems frustrated those efforts. In the end, Yoshida et al. (15) invoked an extended model-free analysis for domain motion that had been previously introduced by Clore et al. (23). They drew two conclusions, subject to the limitations of this model.

First, Yoshida et al. (15) concluded that the RRF flexibility did not substantially alter the interarm angle (our angle θ), so that the overall ''tRNA-mimicking L-shape of RRF (is) maintained.'' Our simulations indicate that, after an initial equilibration period during which θ moves to a new mean value, this is indeed the stiffest degree of freedom for the molecule; this is true for *E. coli* RRF and for both wild-type and mutant *T. thermophilus* RRF.

Second, those authors found that domain 2 wobbles through a cone with a semiangle of $\sim$30° (a full angle of $\sim$60°), and they suggested that the principal mode of motion might be that which corresponds to our angle α, (their Fig. 8). It is interesting to note that this is the same degree of freedom for which we find the largest range of motion in *E. coli* RRF (Fig. 2 *B*). In our model, this angle changes from $\sim -20°$ to $\sim +60°$. We also see a slightly smaller range of motion in β, and the average of these two motions would give reasonably good agreement with the NMR results, if we interpret the combination as filling a cone, and assuming that the RRF molecule continues to diffuse back and forth in both degrees of freedom.

It is also interesting to note that the largest eigenvalue that Yoshida et al. (15) found in their principal component analysis corresponds to a motion that combines our α and β degrees of freedom (their Fig. 2). These are the major motions in our model, too, suggesting that their conclusion that RRF flexibility is essentially due to ''door-like'' motions along α is an oversimplification.

The presence of decyl-β-D-maltopyranoside in the crystal structure of ecRRF (10) appeared to stabilize the 124° angle observed between domain 1 and domain 2. We expected that in simulating ecRRF in the presence decanoic acid, the protein would stay in the open conformation, and that the angle would close in the absence of the lipid. To our surprise, simulations of that structure in complex with and without decanoic acid show that both structures rapidly go to an equilibrium angle of 98°. Thus, decanoic acid does not appear to stabilize the open conformation. Decanoic acid does, however, affect the flexibility of RRF. Compared to ecRRF/DEC, ecRRF is more flexible in rotations of each subunit about its own axis (the α and β modes in Fig. 2, *B* and *C*). Decanoic acid contacts both domain 1 and domain 2, so it may be acting as a sort of ''door stop'', limiting the motions of the domains relative to each other. If the flexibility is important to RRF function, molecules that bind to the pocket between domain 1 and 2 may limit RRF's flexibility and be exploited in drug design.

Toyoda et al. (12) solved the structure of *T. thermophilus* RRF and performed genetic analyses on the functions of loop 1 and loop 2. They found that when wild-type ttRRF is grown in a strain of *E. coli* with an RRF defect, ttRRF is incapable of complementing the phenotype. However, when they mutated residues in the loop regions of ttRRF, they found that the mutants were able to fully complement the ecRRF defect. They postulated that the ability of mutant ttRRF to complement defective ecRRF was due to increased flexibility of the mutant protein. We simulated wild-type ttRRF and ttRRF with Arg-32 in loop 1 mutated to glycine. Contrary to what was expected, ttRRF_R32G was less flexible than wild-type ttRRF in both α and β rotations (Fig. 2, *E* and *F*). However, the difference in global flexibility was modest (Fig. 3). This was shown by the standard deviations of the superposition of each frame of the trajectories onto the respective average structures. The standard deviations were 0.68 and 0.58 Å for ttRRF and ttRRF_R32G, respectively.

Another unexpected finding was that the interdomain angle for ttRRF_R32G oscillated around 78°, which is close to the crystallographic value of 81°, whereas ttRRF moved to an equilibrium value of 118°. Interestingly, the 118° angle of ttRRF is similar to the crystallographic angle for ecRRF in complex with decyl-β-D-maltopyranoside. This suggests that RRFs have both open and closed conformations, and that ttRRF favors the open conformation, whereas ttRRF_R32G, ecRRF, and ecRRF/DEC favor the closed conformation. One possible reason that wild-type ttRRF does not complement mutant ecRRF is that *E. coli* requires RRF to be in the closed conformation.

It would be extremely expensive to carry out molecular dynamics simulations on RRF in situ on the ribosome, and the simulated motions for RRF reported here may be different if they were performed in the presence of the ribosome. Nonetheless, our simulations can be used to suggest how the natural modes of RRF flexibility might favor some interactions with the ribosome over others. This can be done by placing the collection of RRF structures generated in the MD simulation into a rigid model of the ribosome and examining the resulting steric conflicts.

In the absence of a crystal structure of RRF bound to the 70S ribosome, it is not possible to accurately and unambiguously place the ensemble of RRF structures from the simulations into the ribosome. We could generate an ensemble of models based on either the cryo-EM structure (8), or the RRF/50S crystal structure (9). Since those studies reported similar positions for RRF, we chose the latter because of the higher resolution of the structure, and because there is some variability of the location of domain 2 in the cryo-EM structure.

Fig. 4 shows the results of this analysis. The top pair of panels shows that similar contacts are predicted for factor-free ecRRF (*left*) and wild-type ttRRF (*right*) if the models are derived by superposing domain 1. This is reasonable, because we positioned RRF using the crystal structure of the RRF/50S complex (9) (which had been first superposed on the 70S crystal structure (20)), and domain 1 provides the principle contacts in that structure. It is also interesting to note that the interactions of the ribosome with domain 1 are more clearly defined in the cryo-EM structure than are those with domain 2, where two alternative conformations are suggested (8). Both the upper panels show contacts with the base of the L7/L12 stalk, which is the region of the largest conformational change in the cryo-EM structure (8). Contacts are also seen with bridge B2a, which connects helix 69 of the large subunit with helix 44 of the small subunit, not far from the decoding site. Both the cryo-EM structure (8) and the crystal structure (9) showed that RRF binding induces appreciable conformational changes in this part of the ribosome.

The predictions for ecRRF and ttRRF differ substantially when superposition of domain 2 is used to generate the

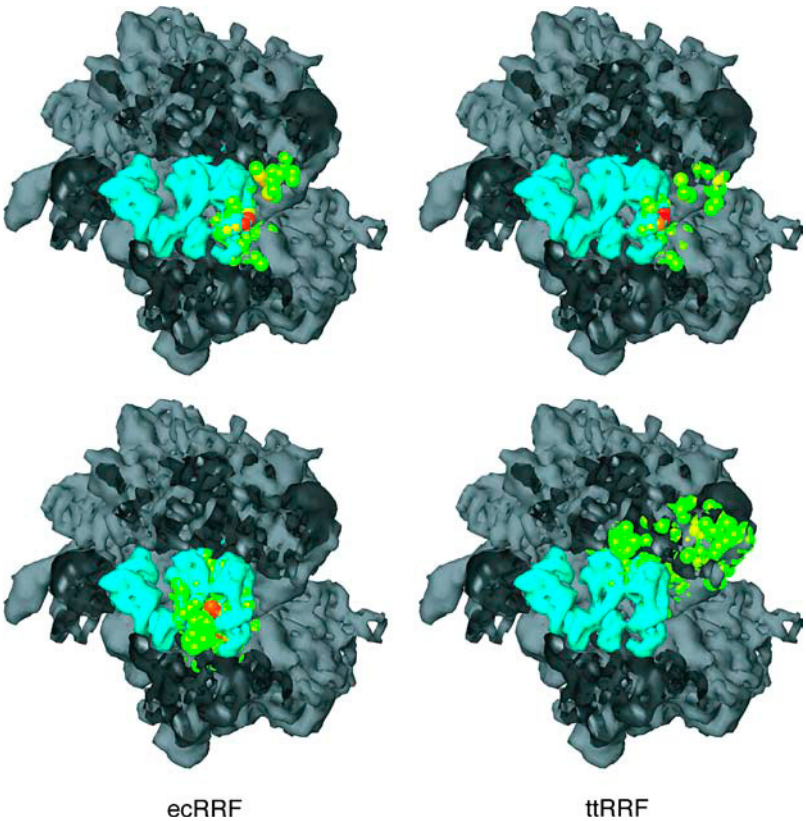

FIGURE 4 Regions of the ribosome that would be contacted by RRF if it were free to adopt the conformations seen in the MD simulations. A cutaway view of the ribosome is shown in gray, seen from above, with the large subunit at the top of each panel, and the small subunit at the bottom. (The projection to the *left* is L1, and the projection to the *right* is the spur; the L7/L12 stalk rises toward the viewer from the *top right-hand* region of the ribosome.) The three tRNAs (*blue*) lie in the intersubunit space and are located at the E-site, P-site, and A-site, from left to right. The top two panels show predictions based on superposition of domain 1 from each panel of the simulation onto domain 1 of the RRF/ribosome model (see Methods), whereas the lower two panels show predictions based on superposition of domain 2. The structures on the left are from simulations of ecRRF without decanoic acid, and those on the right are from wild-type ttRRF. Colored spheres indicate atoms of the ribosome and tRNAs that lie within 5 Å of any RRF atom, and the coloring indicates the frequency of contact, ranging from green (least) through yellow and orange to red (most).

ensemble of models (Fig. 4, *bottom panels*). Domain 2 is substantially smaller than domain 1, so the consequences of the differences in preferred conformations (Fig. 2) are exaggerated when domain 2 is used for superposition. Even so, predictions similar to those of the previous paragraph would result, whether they are based on ecRRF (there are conflicts at bridge B2a), or on ttRRF (which shows conflicts at the base of the L7/L12 stalk). Both ensembles suggest that domain 1 will have steric conflicts with the acceptor terminus of the P-site tRNA. This overlap was among the most important observations of the cryo-EM structure (Agrawal et al., 2004). Those authors suggested that this conflict would lead to the removal of the deacylated P-site tRNA upon EF-G binding; our results suggest that RRF flexibility provides an additional proclivity of RRF to move into the P-site.

In summary, we find that RRF is a highly dynamic protein and that the degree of its flexibility can be influenced by factor binding or by mutations in the hinge region. The presence of decanoic acid inhibited rotations of domain 2 around domain 1 in our simulations, and vice versa for ecRRF. These rotational modes were also inhibited by the R32G mutation of ttRRF. We find that the interdomain bend angle, θ, shows a mixture of open and closed conformations. The simulations of ecRRF start with an angle of 124° (from the crystal structure) and go to an equilibrium value of 98°, whereas the simulation of ttRRF goes to an equilibrium value of 118°, and ttRRF_R32G has an equilibrium value of 77°. Additionally, it is possible that RRF favors two different conformations for rotations of domain 1 around domain 2 and vice versa. When the preferred motions of RRF are mapped onto a rigid model of the ribosome, steric conflicts are produced primarily in those regions where RRF-induced conformational changes have been observed in cryo-EM and in the cocrystal of RRF with the 50S subunit. It is particularly interesting to observe that the natural modes of RRF flexibility favor motions that would tend to push the deacylated tRNA out of the P-site, which has obvious implications for promoting the normal termination of translation. As computational power and molecular dynamics protocols advance, simulations of a fully hydrated ribosome with cofactors may elucidate these detailed molecular mechanisms of translation.

SUPPLEMENTARY MATERAL

An online supplement to this article can be found by visiting BJ Online at http://www.biophysj.org.

This work was supported by National Institutes of Health grant GM53827 to SCH.

REFERENCES

1. Janosi, L., R. Ricker, and A. Kaji. 1996. Dual functions of ribosome recycling factor in protein biosynthesis: disassembling the termination complex and preventing translational errors. *Biochimie*. 78:959–969.
2. Nakamura, Y., and K. Ito. 2003. Making sense of mimic in translation termination. *Trends Biochem. Sci.* 28:99–105.
3. Janosi, L., I. Shimizu, and A. Kaji. 1994. Ribosome recycling factor (ribosome releasing factor) is essential for bacterial growth. *Proc. Natl. Acad. Sci. USA*. 91:4249–4253.
4. Janosi, L., H. Hara, S. Zhang, and A. Kaji. 1996. Ribosome recycling by ribosome recycling factor (RRF): an important but overlooked step of protein biosynthesis. *Adv. Biophys*. 32:121–201.
5. Karimi, R., M. Y. Pavlov, R. H. Buckingham, and M. Ehrenberg. 1999. Novel roles for classical factors at the interface between translation termination and initiation. *Mol. Cell*. 3:601–609.
6. Selmer, M., S. Al-Karadaghi, G. Hirokawa, A. Kaji, and A. Liljas. 1999. Crystal structure of *Thermotoga maritima* ribosome recycling factor: a tRNA mimic. *Science*. 286:2349–2352.
7. Lancaster, L., M. C. Kiel, A. Kaji, and H. F. Noller. 2002. Orientation of ribosome recycling factor in the ribosome from directed hydroxyl radical probing. *Cell*. 111:129–140.
8. Agrawal, R. K., M. R. Sharma, M. C. Kiel, G. Hirokawa, T. M. Booth, C. M. Spahn, R. A. Grassucci, A. Kaji, and J. Frank. 2004. Visualization of ribosome-recycling factor on the Escherichia coli 70S ribosome: functional implications. *Proc. Natl. Acad. Sci. USA*. 101: 8900–8905.
9. Wilson, D. N., F. Schluenzen, J. M. Harms, T. Yoshida, T. Ohkubo, R. Albrecht, J. Buerger, Y. Kobayashi, and P. Fucini. 2005. X-ray crystallography study on ribosome recycling: the mechanism of binding and action of RRF on the 50S ribosomal subunit. *EMBO J*. 24: 251–260.
10. Kim, K. K., K. Min, and S. W. Suh. 2000. Crystal structure of the ribosome recycling factor from Escherichia coli. *EMBO J*. 19: 2362–2370.
11. Yoshida, T., S. Uchiyama, H. Nakano, H. Kashimori, H. Kijima, T. Ohshima, Y. Saihara, T. Ishino, H. Shimahara, K. Yokose, T. Ohkubo, A. Kaji, et al. 2001. Solution structure of the ribosome recycling factor from Aquifex aeolicus. *Biochemistry*. 40:2387–2396.
12. Toyoda, T., O. F. Tin, K. Ito, T. Fujiwara, T. Kumasaka, M. Yamamoto, M. B. Garber, and Y. Nakamura. 2000. Crystal structure combined with genetic analysis of the Thermus thermophilus ribosome recycling factor shows that a flexible hinge may act as a functional switch. *RNA*. 6:1432–1444.
13. Atarashi, K., and A. Kaji. 2000. Inhibitory effect of heterologous ribosome recycling factor on growth of Escherichia coli. *J. Bacteriol*. 182:6154–6160.
14. Fujiwara, T., K. Ito, T. Nakayashiki, and Y. Nakamura. 1999. Amber mutations in ribosome recycling factors of Escherichia coli and Thermus thermophilus: evidence for C-terminal modulator element. *FEBS Lett*. 447:297–302.
15. Yoshida, T., S. Oka, S. Uchiyama, H. Nakano, T. Kawasaki, T. Ohkubo, and Y. Kobayashi. 2003. Characteristic domain motion in the ribosome recycling factor revealed by 15N NMR relaxation experiments and molecular dynamics simulations. *Biochemistry*. 42: 4101–4107.
16. Kalé, L., R. Skeel, M. Bhandarkar, R. Brunner, A. Gursoy, N. Krawetz, J. Phillips, A. Shinozaki, K. Varadarajan, and K. Schulten. 1999. NAMD2: greater scalability for parallel molecular dynamics. *J. Comput. Phys.* 151:283–312.
17. Brooks, B. R., R. E. Bruccoleri, B. D. Olafson, D. J. States, S. Swaminathan, and M. Karplus. 1983. CHARMM: a program for macromolecular energy, minimization, and dynamics calculations. *J. Comput. Chem.* 4:187–217.
18. Darden, T., D. York, and L. Pederson. 1993. Particle mesh Ewald. An N·log(N) method for Ewald sums in large systems. *J. Chem. Phys*. 98:10089–10092.
19. Berendsen, H. J. C., J. P. M. Postma, W. F. van Gunsteren, A. DiNola, and J. R. Haak. 1984. Molecular dynamics with coupling to an external bath. *J. Chem. Phys*. 81:3684–3690.

20. Yusupov, M. M., G. Z. Yusupova, A. Baucom, K. Lieberman, T. N. Earnest, J. H. Cate, and H. F. Noller. 2001. Crystal structure of the ribosome at 5.5 A resolution. *Science*. 292:883–896.

21. Braddock, D. T., J. M. Louis, J. L. Baber, D. Levens, and G. M. Clore. 2002. Structure and dynamics of KH domains from FBP bound to single-stranded DNA. *Nature*. 415:1051–1056.

22. Baber, J. L., A. Szabo, and N. Tjandra. 2001. Analysis of slow interdomain motion of macromolecules using NMR relaxation data. *J. Am. Chem. Soc*. 123:3953–3959.

23. Clore, G. M., A. Szabo, A. Bax, L. E. Kay, P. C. Driscoll, and A. M. Gronenborn. 1990. Deviations from the simple two-parameter model-free approach to the interpretation of nitrogen-15 nuclear magnetic relaxation of proteins. *J. Am. Chem. Soc*. 112:4989–4991.